# Understanding Europium and Terbium Speciation and Ion Pairing in Carbonate Complexes Using Advanced Spectroscopy Techniques

**Hege, Poore, Galley, Reinhart, Jackson, Tian, Shafer**

**Understanding Europium and Terbium Speciation and Ion Pairing in Carbonate Complexes Using Advanced Spectroscopy Techniques**

Nicole Hege,[1] Andrew T. Poore,[2] Shane S. Galley,[1] Benjamin J. Reinhart,[3] Jessica A. Jackson,[1] Shiliang Tian,[2] Jenifer C. Shafer[1]*

[1]Department of Chemistry, Colorado School of Mines, Golden Colorado 80401, United States

[2]Department of Chemistry, Purdue University, West Lafayette, Indiana 47906, United States

[3]Advanced Photon Source, Argonne National Laboratory, Lemont, Illinois 60439, United States

[*]Applied Chemistry Program, Colorado School of Mines, Golden, Colorado 80401, United States. E-mail: jshafer@mines.edu

ORCID iD: Hege 0000-0002-6649-7465; Poore 0009-0007-1650-0471; Galley 0000-0003-0679-6567; Reinhart 0000-0001-5654-8823; Jackson 0000-0002-6567-2495; Tian 0000-0002-9830-5480; Shafer 0000-0001-9702-1534

Keywords: Carbonate, EXAFS Spectroscopy, Ion pairing, Lanthanides, XANES Spectroscopy

# Abstract

The lanthanide (Ln) elements are critical materials that are typically extracted/mined together. Their separation by use of solvent extraction from acidic media is well known; however, there are few studies in basic media with carbonate anions. We investigated the complexation of Eu(III) and Tb(III) carbonates as solids and solutions in alkaline $K_2CO_3$, wherein we sought to access a Tb(IV) carbonate complex through ozonolysis. $L_3$-edge XANES of Eu and Tb carbonate solids, colorless solutions, and a red-hued Tb solution (obtained by ozonolysis) all showed Ln(III) cations. The absence of evidence for a Tb(IV) complex was confirmed through XAS and EPR analyses, despite the solution exhibiting a deep red color. For solids and solutions, EXAFS results indicate molecular Ln(III)-carbonato anions. In terms of the Eu(III) carbonate coordination number, the coordination does not change upon dissolution of the solid sample. Furthermore, EXAFS for the solutions revealed evidence for the association of potassium cations with the Ln(III)-carbonato anions. This direct observation of contact ion pairing by EXAFS at room temperature is rare. The insights into Ln(III) carbonate complexation and solution speciation afforded by XANES-EXAFS, FT-IR, and EPR provides perspectives that serve as benchmarks for future computational and experimental efforts focused on caustic-side solvent extraction of Ln(III) ions.

# Introduction

The lanthanide (Ln) elements exhibit a range of uses, including luminescent materials, magnets, catalysts, MRI contrast agents, and radiopharmaceuticals.[1–3] For these (and other) applications, the extraction and separation of individual lanthanides is vital to the global energy economy as well as life and medical sciences alike. The chemical, physical, and structural properties of the lanthanides are very similar across the period and, moreover, the 4f electrons do not participate in ligand bonding, making the Ln elements difficult to separate using typical chemical separations, such as liquid-liquid extraction or fractional crystallization.[4] The dissolution of ore minerals and their treatment in hydrometallurgical processes using aqueous solutions of acidic and alkaline nature are vast commercial enterprises with environmental implications. For example, although solvent extraction from acidic media is common,[5] the mineral industry is facing regulatory pressures to reduce liquid acid wastes.[6] Alternative approaches that have not been studied extensively but that show promise include the use of basic carbonate media instead of acidic media. The unique feature of carbonate media is that—while Ln (III) ions typically precipitate out of alkaline solutions—some Ln (III) ions remain in alkaline carbonate solutions as anionic carbonate complexes, which allows liquid-liquid separations processes to be explored.[7] One such approach involves the isolation of Ln elements in waste streams that are produced as a byproduct of phosphogypsum manufacturing, involving high concentrations of ammonium carbonate. Litvinova et al. focused their thermodynamic studies on Nd, Sm, Gd, and Ho carbonate-alkali containing systems concluding that a REE bicarbonate complex was most favored over other investigated complexes,[8] while De Vasconcellos et al. studied the separation of $Y_2O_3$ from a wide range of Ln carbonates, including La, Ce, Pr, Nd, Sm, Gd, and Dy.[9] They were able to achieve a separation for $Y_2O_3$ of 81% with two steps. Additionally, Bruckner and colleagues were able to achieve an 80% recovery of the Ln elements in gypsum using carbonate media which was abundant in three lanthanides (i.e., La, Ce, and Nd).[10] Another Ln separation approach involved the dissolution of basic rare earth carbonates in potassium carbonate solutions that were processed through an anion exchange resin, Dowex 1.[11,12] The success of the method hinges upon the formation of anionic carbanoto complexes in alkaline solutions of concentrated $K_2CO_3$.[13] Moreover, it turns out that concentrated alkaline carbonate solutions facilitate the oxidation of trivalent Ce[14,15] and, possibly even Pr (III) and Tb (III).[15–19] In fact, the ozonolysis of Tb (III) periodate in an aqueous alkaline solution appears to provide an entry to the solvent extraction of an anionic Tb (IV) periodate complex with quaternary amines, like Aliquat 336.[20] Such a manipulation of the oxidation state presents an opportunity to devise high performance separation techniques for neighboring lanthanides.

Tetravalent Ln oxidation states are of interest to chemical separations because there are just three lanthanides that are known to exist in that state, which would be readily extracted from all trivalent ions. Cerium (IV) is renowned and well established.[21–24] The other lanthanides that can have a tetravalent oxidation state, most exclusively in the solid state, are praseodymium and terbium.[25] The stabilization of transient solution species of Pr (IV) and Tb (IV) in aqueous media

is a challenge for the conventional liquid-liquid extraction processes. Nonetheless, the ozonolysis and electrolysis of Tb (III) solutions in alkaline electrolytes with high carbonate concentrations appear to provide an entry to what may well be Tb (IV) carbanoto complex anions. There is agreement in the literature about the dark red- and red-brown-hued colors that result upon the ozonolysis and electrolysis of clear and colorless Tb (III) carbonate solutions.[14,15,17–19] Despite the generally broad and nondescript nature of the optical spectra of these solutions as well as bulk measurements of currents and voltages, many articles suggest that this color change is proof of the presence of Tb (IV).[14,16] There is little direct information about the redox speciation of the Tb ions in these red-hued carbonate solutions, such as is available by use of electron paramagnetic resonance (EPR) and Tb $L_3$-edge X-ray absorption spectroscopy (XAS). XAS—including XANES and EXAFS—can also provide direct element specific insights into the nature of the limiting solution speciation in highly alkaline-carbonate complexes.

Although, the structures of solid-state lanthanide (III) carbonates have been studied definitively,[26–30] the nature of the limiting speciation of Ln (III) carbonate complexes in solution is less definitive, despite extensive experimental and computational research.[8,31–33] For example, Taravel et al. suggested a general formula of $[Ln(CO_3)_x(H_2O)_y]^{z-}$ for di-, tri- and tetracarbonates (x = 2, 3, 4; z = 1, 3, 5, respectively).[34] Subsequent experimental studies by Philippini et al. have focused on determining the stabilization for tri- and tetra-carbonates with heavier lanthanides and lighter lanthanides, respectively.[35,36] Furthermore, quantum chemical modeling results[15,32] reveal the tetracarbonate anion in agreement with the speciation deduced from experimental studies.[37,38] Despite these efforts, and in view of the sixteen different carbonate bonding modes (mono-dentate, bi-dentate, bridging, etc.[39]) and varying extents of hydration,[32] the issue of limiting speciation is still relevant today.

We report new knowledge obtained through XAS, EPR, and FT-IR about the carbonate speciation of two elements near the center of the 4f period, Eu and Tb. We interrogated the white solids and colorless solutions for both Eu and Tb as well as the red-hued solution of Tb that was obtained following ozonolysis. The $L_3$-edge XANES studies revealed Eu (III) and Tb (III) ions for all samples. Remarkably, following ozonolysis of the alkaline Tb (III)-$K_2CO_3$ solution system, we found no indication for Tb (IV) in the red-hued solution. Only Tb (III) was detected by XANES and EPR spectroscopy, and the FT-IR data indicated a hydroxo-carbonato-complex. Being separated by just one element (Gd), the Eu and Tb $L_3$-edge EXAFS studies revealed subtle, yet unanticipated, differences in speciation in solution, involving the formation of anionic coordination complexes with trivalent Eu and Tb. Additionally, we found evidence that the anionic carbonate complexes in the colorless Eu (III) and Tb (III) solutions are associated with potassium ions, most likely in the form of cation contact ion-pairs.[40,41]

# Results

## XANES

***Solid versus solution structures.*** The Ln $L_3$-edge XANES for the Eu and Tb carbonate complexes as solid salts and as salts dissolved in aqueous, alkaline 5.5 M $K_2CO_3$ solutions are shown in Figures 3a and 4a, respectively. The intense edge peaks at approximately +3.0 eV with Lorentzian line-shapes having full widths at half-maximum (fwhm) of 5-7 eV are typical for the trivalent lanthanide ions (Table S1 and S2).[42] These peaks are due to electronic transitions from the Ln $2p_{3/2}$ initial states to the empty 5d orbitals, which are affected by the O ligand field about the Ln ions.[43–45] To aid in the observation of unresolved edge features in the primary XANES, the second derivative XANES data is often calculated to minimize the contribution of the steplike arctangent response that contributes to the asymmetry of the edge peak on the high-energy side.[46] The second derivative Eu and Tb XANES data for the solid salts and their solutions are shown in Figures 3b and 4b, respectively. In these—with one exception—the response appears as symmetrical, concave peaks with the same relative intensities and positions as the original Lorentzians.[42] The fwhm for both solutions are equivalent (5.3 eV) and narrower than the fwhm for both solids (6.3 eV), which are also equivalent (Table S1). Such information signifies a change in speciation upon dissolution of the solid salts in 5.5 M $K_2CO_3$. This speciation change will be discussed further in the EXAFS analyses.

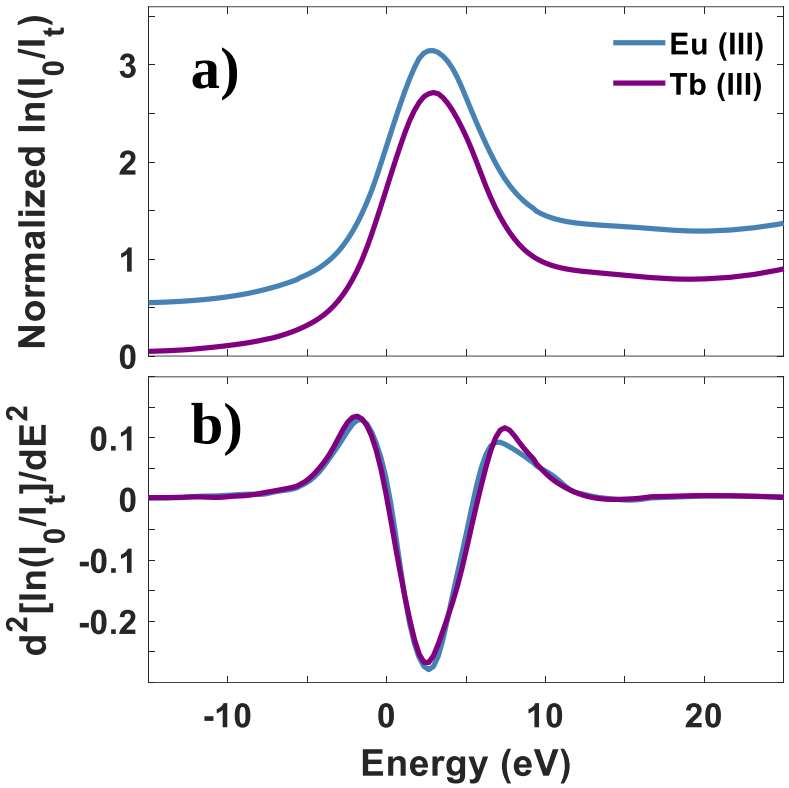


Figure 3: (a) Normalized Eu and Tb $L_3$-edge XANES for the white solid carbonate salts showing the data rescaled to the inflection point energies (Table S3) and offset for clarity. The edge peak maximums and Lorentzian fwhm are reported in the SI (Tables S1 and S2). (b) The second derivative data of the XANES in part (a).

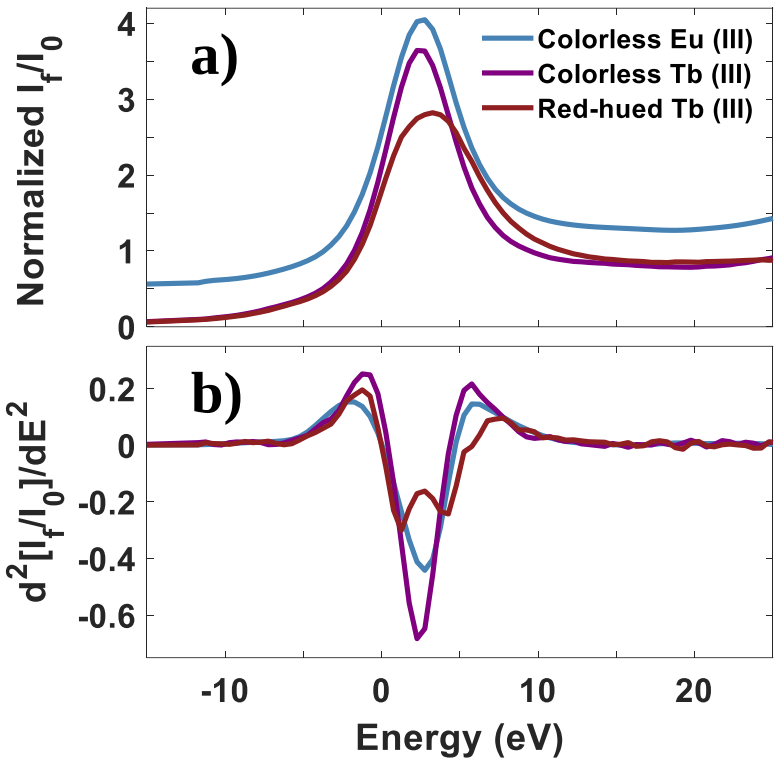


Figure 4: (a) Normalized Eu and Tb $L_3$-edge XANES for the two colorless carbonate solutions and the one red-hued Tb carbonate solution showing the data rescaled to the inflection point energies (Eu offset for clarity, Table S3). The edge peak maximums and Lorentzian fwhm are listed in the SI (Tables S1 and S2) (b) The second derivative data of the XANES in part (a).

***Terbium-$K_2CO_3$-$O_3$ solution system.*** The data for the red-hued Tb solution in 5.5 M $K_2CO_3$ following ozonolysis is the exception (Figure 4a). The fwhm is the broadest (7.0 eV). The peak breadth arises from a combination of two unresolved Lorenztian edge peaks. The 2$^{nd}$ derivative XANES resolves the two peaks (Figure 4b)—and so does the edge peak fitting (Figure S8, Table S2, and Table S16)—revealing a peak-to-peak separation of 3.0 eV. This value of 10 *Dq* (3 eV) is typical of that seen for Ln (III) ions in an octahedral field of 6 O atoms.[43,46] This doublet in the second derivative XANES arises from the dipole allowed electronic transitions from the Tb (III) 2p initial state to the empty 5d $t_{2g}$ state (7517 eV) and to the empty 5d $e_g$ state (7520 eV).[44,45] The 3-eV difference between these $t_{2g}$ and $e_g$ electronic states corresponds to 413 nm. This wavelength contributes to the broad absorption maxima of UV-Vis spectra obtained for Tb (III) solutions following ozonolysis and electrolysis reported in the literature[15–17] as well as for the optical spectrum obtained in this study (Figure 1). No such ligand field splitting is resolved in the second derivative XANES for the four other specimens, indicating that the O coordination environments are not octahedral. This is consistent with the EXAFS analysis described in the next section.

Unlike Tb $L_3$-edge XANES, which is a direct, element-specific probe of Tb valence and coordination, the largely nondescript UV-vis response of the red-hued terbium solution complex (Figure 1) may arise from electronic transitions not directly associated with Tb. In contrast to all previous reports suggesting the production of Tb (IV) by the action of ozone in alkaline carbonate containing electrolytes, our Tb XANES evidence reveals only Tb (III). The absence of a response typical of Tb (IV) may be due to the low $OH^-$ concentration (0.1 M). Previous research suggests that approximately 0.2 M hydroxide concentration is necessary to oxidize Tb (III) with ozone.[19] Nonetheless, the color of the ozonized Tb (III) solution still presents a quandary because the observed color is frequently associated with the presence of Tb (IV), which isn't found in the solution. Specifically, our XANES data do not exhibit the Tb (IV) response as seen in the $TbO_2$[47], $BaTbO_3$[48], and $SrTbO_3$[48–50] literature standards. Figure 5 shows representative XANES for valence pure compounds of Tb (III) and Tb (IV) and a mixed valence (Tb (III)-Tb (IV)) oxide. Coincidentally, electrolysis experiments also produce red-hued Tb solutions and optical spectra essentially identical to our response of Figure 1.[14–16,19]

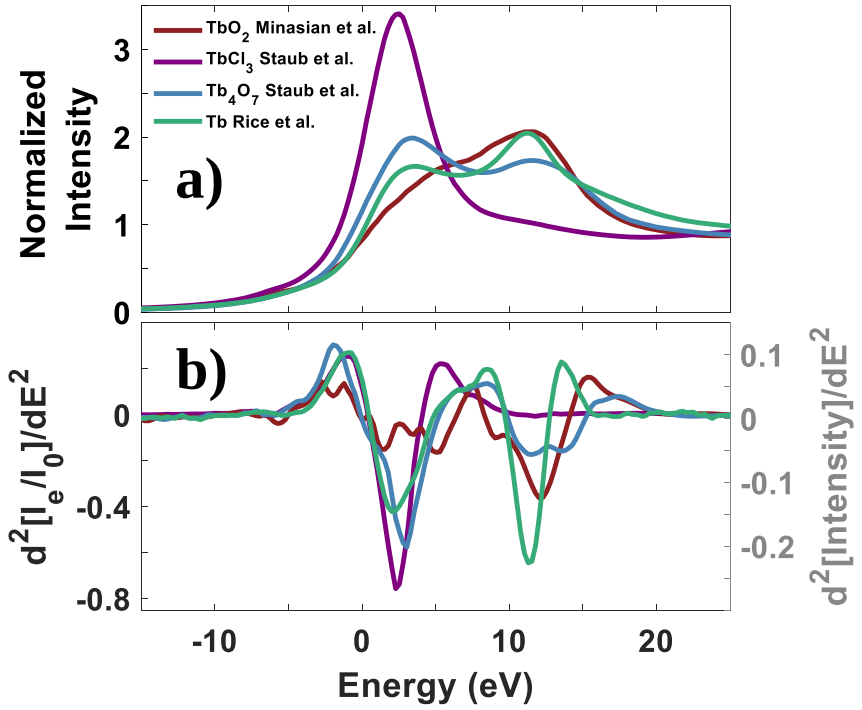


Figure 5: (a) Normalized Tb $L_3$-edge XANES for the solid materials of valence-pure $Tb(III)Cl_3$ and mixed valence $Tb(III/IV)_4O_7$ of Staub et al.[50], the tetrahedral Tb (IV) complex [Tb(NP(1,2-bis-tBu-diamidoethane)($NEt_2$))$_4$] of Rice et al.[51], and for $Tb(IV)O_2$ of Minasian et al.[47] The data have been rescaled using the inflection point energies (Table S3). The edge peak maxima in Table S2. (b) The second derivative data of the XANES in part (a). The $Tb(III)Cl_3$ data is plotted on the left y-axis and all three other data sets are scaled using the right y-axis for comparison.

To further investigate the oxidation state of Tb in the red-hued solutions, EPR spectra for both colorless and red-hued solutions were recorded (Figure S6). Tb (IV), with its $4f^7$ electronic configuration, forms an S=7/2 Kramers ion. This configuration results in substantial zero field splitting (ZFS), which distinctly separates the energy levels across the spin projection ($m_s$) levels, leading to complex EPR spectra characterized by highly anisotropic g values.[51–54] Notably, a strong spectral feature at approximately g≈5 has been identified and attributed to transition within the $m_s = \pm 3/2$ doublet.[51] In contrast, Tb (III), with its $4f^8$ electronic configuration, does not exhibit the intense EPR features, as expected for the S=3 non-Kramers ion. Although integer spin systems usually produce stronger signals in parallel mode EPR, Tb (III) complexes can still be detected in the more conventional perpendicular mode, displaying features at low magnetic fields corresponding to very large $g_{//}$ values (17.8-10.44).[55] As shown in Figure S6, the observed EPR spectra for both the colorless and red-hued solutions demonstrate signals only below 700 G. EasySpin simulations of these spectra indicate a $g_{//}$ of approximately 17.0, consistent with previously reported Tb (III) species.[55,56] This suggests that the red-hued solution predominantly contains Tb (III), aligning with the findings from the XANES studies. The feature around 2000 G is hard to determine amongst the resolution of the EPR spectrum; therefore, speculation of the possible origin of this feature can be found in the SI.

## EXAFS

The Eu and Tb $k^3\chi(k)$ EXAFS and the corresponding Fourier transform (FT) data for the solid salts and their solutions in 5.5 M $K_2CO_3$ are shown in Figures 6 and 7 as solid lines. The one-shell (Ln-O) fits to the Tb and Eu solid and liquid $k^3\chi(k)$ EXAFS and their corresponding FT data are shown in the SI (Figures S2-S3 and Table S9). The stepwise addition of coordination shells beyond the innermost Ln-O shell provides statistically significant improvements in the fits, indicating that—even though the nearest O backscattering dominates the experimental EXAFS as illustrated by the intense Ln-O peaks in the FT data—the scattering from the C and distal O atoms of the carbonate anions in bidentate and monodentate coordination as well as backscattering by outer sphere metal cations has a significant effect on the response, see Tables 1 and 2.[27,31,57] Structure complexation diagrams for all 5 samples are illustrated in Figure 8.

### *Europium-$O_9$ versus terbium-$O_8$ coordination.*

**Solids.** The numerical results of Table 1 for the Eu (III) solid salt reveal a total nearest O CN = 9 as well as approximately 2 distant $C_b$ and $O_{dis}$ atoms and 4 distant $C_m$ atoms. These results indicate that the Eu solid exhibits two bidentate carbonates and four monodentate carbonates, accounting for 8 of the 9 O atoms. The other inner sphere O atom must arise from either hydroxide or water coordination as, for example, $[Eu(CO_3)_6(H_2O)]^{9-}$ or $[Eu(CO_3)_6(OH)]^{10-}$. Because the backscattering by O from $OH^-$ and $H_2O$ is indistinguishable within the resolution of our EXAFS, the most accurate description of the complex stoichiometry can only be provided in general terms as $[Eu(CO_3)_6(OH_n)]^{(y-9)}$ for n = 1,2, y = n-2. In the alkaline carbonate solutions employed for

synthesis, the $OH^-$ anion could be more competitive compared to water coordination. The EXAFS data also revealed the association of approximately 4 $Na^+$ ions in the outer sphere of the heteroleptic molecular anion.

The numerical results for the Tb (III) solid salt (Table 1) reveals a total innermost O CN of 8. Four of these are attributed to the bonding of two bidentate and three monodentate carbonates, based on the $C_b$ and $O_{dis}$ CN of approximately 2 and $C_m$ of 3. The remaining O atom is accounted for by either hydroxide and/or water coordination as, $[Tb(CO_3)_5(OH_n)]^{(y-7)}$ for n = 1,2, y = n-2. We found evidence that this heteroleptic molecular anion associates with approximately 2 distant $Na^+$ ions. In each solid, we found evidence for contact ion pairing with 4 and 2 $Na^+$ ions in the outer spheres of the Eu and Tb molecular anions, respectively. For the innermost O sphere, there is a 0.066 Å difference between the 2.438 Å Eu-$O_9$ and 2.372 Å Tb-$O_8$ distances (Table 1). Table 1 also shows that the bidentate Eu-$C_b$ and Tb-$C_b$ distance difference is 0.05 Å, monodentate Eu-$C_m$ and Tb-$C_m$ distance difference is 0.09 Å, the Eu-$O_{dis}$ and Tb-$O_{dis}$ distance difference is 0.025 Å, and the Eu-Na and Tb-Na distance difference is 0.10 Å.

**Solutions.** According to the mixed bidentate and monodentate model fit (Figure 2 and Table 2) of the Tb $k^3\chi(k)$ EXAFS (Figure 7) for the colorless solution, the results suggest a homoleptic $[Tb(CO_3)_4]^{5-}$ anion with approximately 6 outer sphere potassium cations. All 8 of the innermost O atoms are accounted for by four bidentate carbonate anions, confirming the result of Janicki et al,[26] that terbium forms an eight coordinate $[Tb(CO_3)_4]^{5-}$ complex in solution. Dissimilarly, the Eu $k^3\chi(k)$ EXAFS (Figure 7) were fit to reveal a homoleptic complex in which all 9 innermost O are accounted for by a mixed 3 bidentate and 3 monodentate carbonate anions as $[Eu(CO_3)_6]^{9-}$. We found evidence that approximately 5 distant $K^+$ ions are associated with this anion complex. For the innermost O sphere, there is a 0.038 Å difference between the 2.431 Å Eu-$O_9$ and 2.393 Å Tb-$O_8$ distances (Table 2). Table 2 also shows that the bidentate Eu-$C_b$ and Tb-$C_b$ distance difference is 0.041 Å, the Eu-$O_{dis}$ and Tb-$O_{dis}$ distance difference is 0.170 Å, and the Eu-K and Tb-K distance difference is 0.050 Å.

Table 1: Multi-shell Ln (III) EXAFS fit summary of solid sodium salts of the Tb (III) and Eu (III) carbonate complexes given a mixed bidentate and monodentate carbonate coordination model with SS and MS paths. Errors are reported in parentheses at the 95% confidence level.

| Sample | Scattering Path | Number of Coordinating Atoms | Distance of Coordinating Atoms, r (Å) | Debye-Waller Factor, $\sigma^2$ ($Å^2$) | $E_0$ (eV) | *R*, % |
|---|---|---|---|---|---|---|
| $Eu^{3+}$ Solid | Eu-O | 9.2 (5) | 2.438 (4) | 0.0116 (1) | 2.8 (1) | 2.6 |
| | Eu-$C_b$ | 1.8 (1) | 2.92 (1) | / | / | |
| | Eu-$C_m$ | 4.2 (4) | 3.6 (1) | / | / | |
| | Eu-$O_{dis}$ | 1.8 (1)* | 4.075 (9) | / | / | |
| | Eu-Na | 4.0 (3) | 4.28 (1) | / | / | |
| | Eu-$C_b$-$O_{dis}$ | 1.8 (1)* | 4.075 (9)* | / | / | |
| | Eu-$C_b$-$O_{dis}$-$C_b$ | 1.8 (1)* | 4.075 (9)* | / | / | |
| $Tb^{3+}$ Solid | Tb-O | 8.4 (7) | 2.372 (6) | 0.0110 (1) | 2.7 (4) | 4.3 |
| | Tb-$C_b$ | 2.4 (2) | 2.87 (2) | / | / | |
| | Tb-$C_m$ | 2.9 (7) | 3.51 (2) | / | / | |
| | Tb-$O_{dis}$ | 2.4 (2)* | 4.10 (1) | / | / | |
| | Tb-Na | 2.1 (6) | 4.18 (3) | / | / | |
| | Tb-$C_b$-$O_{dis}$ | 2.4 (2)* | 4.10 (1)* | / | / | |
| | Tb-$C_b$-$O_{dis}$-$C_b$ | 2.4 (2)* | 4.10 (1)* | / | / | |

*Linked with corresponding Ln-$C_b$ coordination value or Ln-$O_{dis}$ distance value.

/ Linked with previous value.

Fit residual according to WinXAS output.[58,59]

Table 2: Multi-shell Ln (III) EXAFS fit summary with SS and MS paths for the potassium salts of the Ln carbonate solution complexes dissolved in 5.5 M $K_2CO_3$. Errors are reported in parentheses at the 95% confidence level.

| Sample | Scattering Path | Number of Coordinating Atoms | Distance of Coordinating Atoms, r (Å) | Debye-Waller Factor, $\sigma^2$ ($Å^2$) | $E_0$ (eV) | *R*, % |
|---|---|---|---|---|---|---|
| $Eu^{3+}$ Colorless Solution | Eu-O | 8.7 (4) | 2.431 (3) | 0.0075 (1) | 1.5 (1) | 3.7 |
| | Eu-$C_b$ | 3.2 (1) | 2.911 (7) | / | / | |
| | Eu-$C_m$ | <u>3</u> | 3.63 (3) | / | / | |
| | Eu-$O_{dis}$ | 3.2 (1)* | 4.04 (1) | / | / | |
| | Eu-K | 5.1 (4) | 4.01 (1) | / | / | |
| | Eu-$C_b$-$O_{dis}$ | 3.2 (1)* | 4.04 (1)* | / | / | |
| | Eu-$C_b$-$O_{dis}$-$C_b$ | 3.2 (1)* | 4.04 (1)* | / | / | |
| $Tb^{3+}$ Colorless Solution | Tb-O | 7.6 (8) | 2.393 (6) | 0.0071 (2) | 2.7 (3) | 5.7 |
| | Tb-$C_b$ | 4.2 (6) | 2.87 (1) | / | / | |
| | Tb-$O_{dis}$ | 4.2 (6)* | 3.87 (2) | / | / | |
| | Tb-K | 4.4 (9) | 3.96 (2) | / | / | |
| | Tb-$C_b$-$O_{dis}$ | 4.2 (6)* | 3.87 (2)* | / | / | |
| | Tb-$C_b$-$O_{dis}$-$C_b$ | 4.2 (6)* | 3.87 (2)* | / | / | |
| $Tb^{3+}$ Red-Hued Solution | Tb-O | 6.3 (4) | 2.274 (3) | 0.0061 (1) | 0.7 (2) | 5.2 |
| | Tb-$C_m$ | 2.7 (3) | 3.29 (1) | / | / | |
| | Tb-K | 0.6 (1) | 3.8 (1) | / | / | |
| | Tb-$O_{m2}$ | 2.5 (5) | 4.18 (2) | / | / | |

*Linked with corresponding Ln-$C_b$ coordination value or Ln-$O_{dis}$ distance value.
/ Linked with previous value.
Underlined; Value was fixed to satisfy the condition where Eu-O= 2 $C_b$ + 1 $C_m$.
Fit residual according to WinXAS output.[58,59]

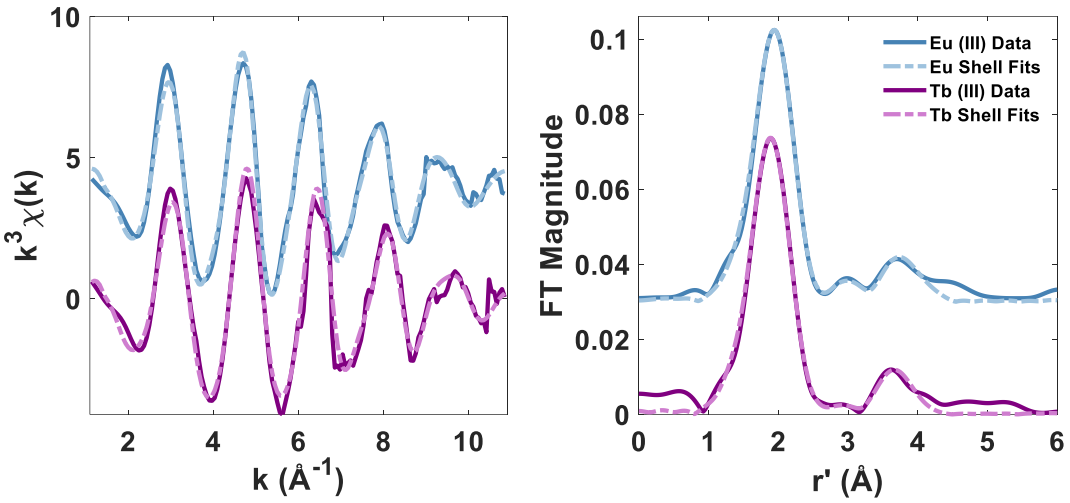


Figure 6: The $k^3\chi(k)$ EXAFS and the corresponding FT data for the white Eu (III) and Tb (III) carbonate solid samples as sodium salts. The Eu data sets are arbitrarily offset for clarity.

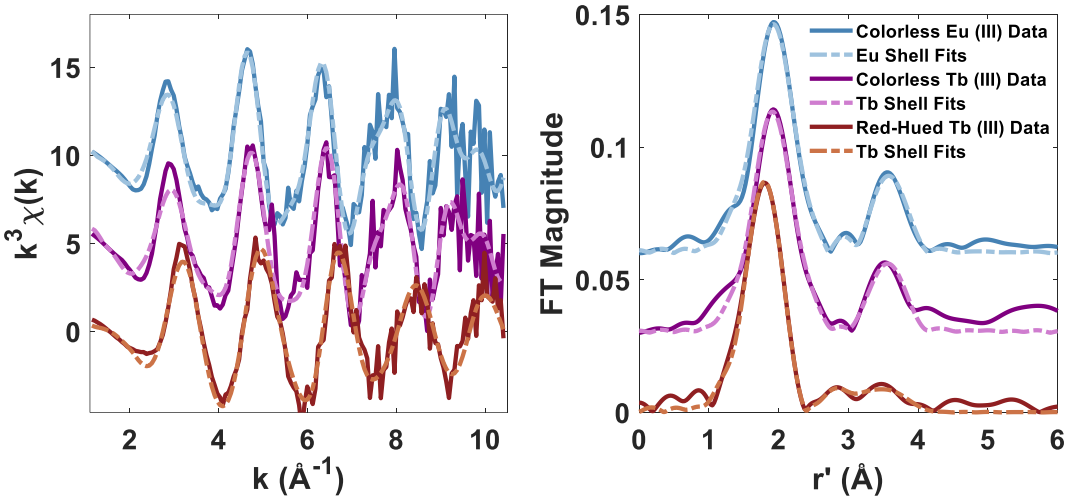


Figure 7: The $k^3\chi(k)$ EXAFS and the corresponding FT data for the colorless solutions of the Eu (III) and Tb (III) carbonate complexes as well as the red-hued Tb (III) complex in potassium salts dissolved in 5.5 M $K_2CO_3$. EXAFS data for both Eu and Tb colorless data sets are arbitrarily offset for clarity.

***Solid versus solution structures.*** The results (Tables 1 and 2) for the inner-sphere Eu-O coordination indicate 9 O atoms at an average of 2.43–2.44 Å for both the white sodium salt and the colorless solution obtained by dissolution. The inner-sphere Tb-O coordination for both the white sodium salt (2.37 Å) and the colorless solution (2.39 Å) is shown to involve 8 O atoms at an average distance of approximately 2.38 Å. The 0.05–0.06 Å distance difference is readily accounted for by the effects of the Ln contraction and different O CNs. If the Eu and Tb O CNs were the same (either 8 or 9), then, based upon ionic radii arguments alone, the distance difference would amount to only 0.026 Å.[60] As amplified in the Discussion section, by accounting for the 1

O difference in the CNs, the ionic radii predict that a larger distance difference, 0.08 Å, is obtained, which is in accordance with the EXAFS-determined results.

Although weak, the peaks beyond the intense Ln-O peaks observed in the FT data for the Eu and Tb solids (Figure 6) are of physical significance in terms of carbonate anion and sodium cation backscattering. Upon the dissolution of the solid salts in 5.5 M $K_2CO_3$, the most distant peaks in the FT data become more pronounced (Figure 6). Whether this intensification is structural in origin or simply reflects the fact that K has a stronger backscatter than Na (Figure S5), is open to discussion. To address this issue regarding the prominent distant peaks (at approximately 3.9 Å before phase shift correction) in the solution FTs, multi-shell, and best-Z fitting were performed for the solid materials and solution samples. The results of Tables 1 (solids) and 2 (solutions) are based upon the mixed bidentate and monodentate coordination model for carbonate, wherein the number of $C_b$ atoms and the number of $O_{dis}$ atoms are equivalent. The coordination numbers indicate that there is more bidentate carbonate complexation (1-2 anions) to the Eu and Tb ions in solution compared with that (2 bidentate anions) for the solid materials. Moreover, the complexation response includes contributions from Ln-Na ($Na_2CO_3$ solids) and Ln-K ($K_2CO_3$ solutions) correlations.

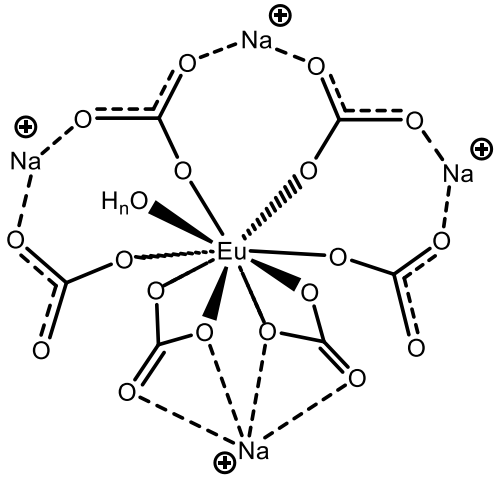


(a) Eu (III) Solid

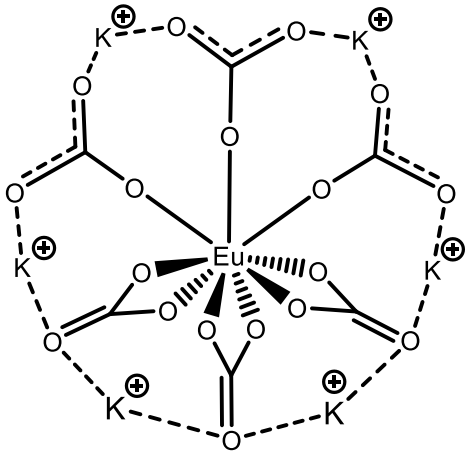


(b) Eu (III) Colorless Solution

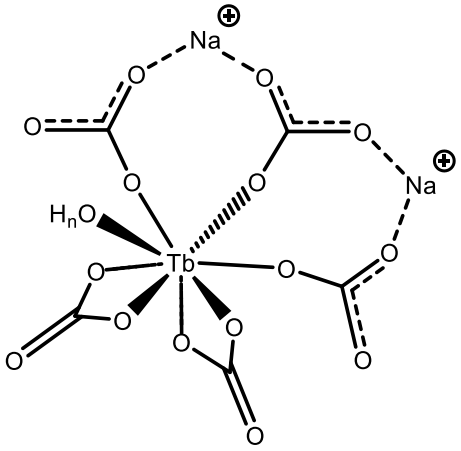


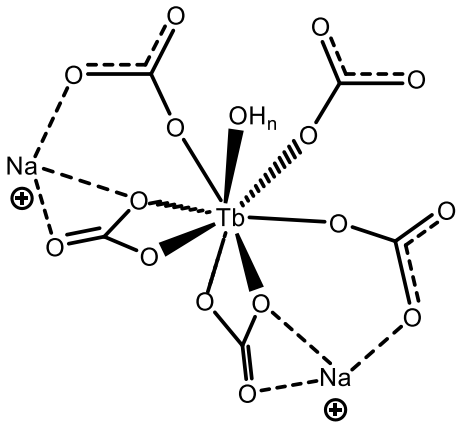


(c) Tb (III) Solid

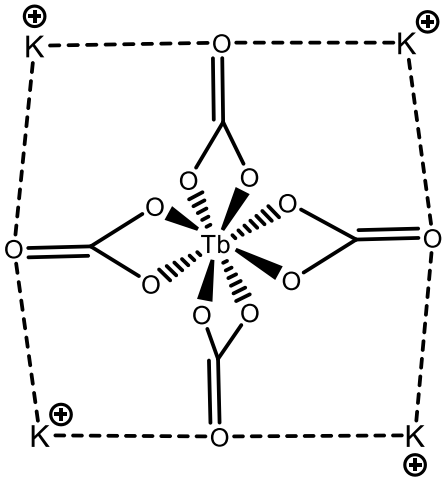


(d) Tb (III) Colorless Solution

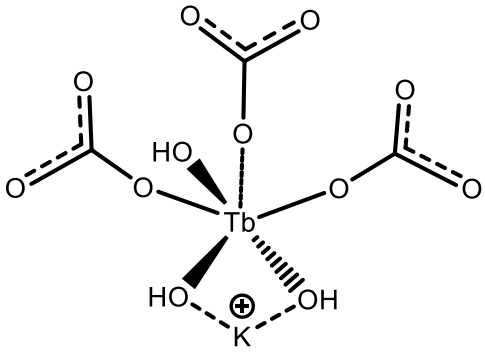


(e) Tb (III) Red-Hued Solution

Figure 8: Structures created from the results in Tables 1 and 2, where the cation positions are estimated using information from Table S10.

***Terbium-$K_2CO_3$-$O_3$ solution system.*** For the red-hued Tb (III) solution, there is a reduced O coordination number of approximately 6, which is consistent with the XANES response and unlike the 8 O-coordinate Tb (III) ions in the colorless solution. In agreement with the lower O CN, the Tb (III)-O bond length is much shorter at 2.27 Å, Table 2, which amounts to a 0.12 Å contraction of the Tb (III)-O bond length for the colorless solution. We further note that visual and spectroscopic examination of the red-hued terbium solution before and after XAS data acquisition revealed no change in the color. We have no evidence for photoreduction of Tb (IV) to Tb (III), which would result in a bleached-out color following the 3-hour X-ray exposure on the bending magnet beamline during data acquisition. Furthermore, during the time between the completion of ozonolysis at Mines to data acquisition at the APS, the solution color did not fade or change, and no precipitation or turbidity was observed. The XAS results indicate that the red color of the Tb solution produced in our experiments by exhaustive ozonolysis of a Tb (III) carbonate solution is not diagnostic of Tb (IV). Rather, the XANES, EPR, and EXAFS reveal that the solution contains Tb (III) in a unique coordination environment, an observation which will be expanded upon further in the Discussion section.

In the FT data for the red-hued Tb solution, weak features are found beyond the intense Tb (III)-$O_6$ peak. The multishell fitting analysis, Table 2, reveals 6 inner-sphere O atoms and approximately three monodentate carbonate anions, with their associated $C_m$ atoms, accounting for 3 of the 6 nearest O atoms. The core structure of the heteroleptic molecular anion is consistent with the general stoichiometry of $[Tb(CO_3)_3(OH_n)]^{(y-3)}$ for n = 1,2, y = n-2. This anionic complex has approximately one distant K ion correlation at 3.8 Å consistent with contact ion pairing.

To further investigate what is responsible for the color in the red-hued Tb (III) solution, infrared (FT-IR) spectroscopy was measured for both colorless and red-hued Tb (III) solution samples. In figure 9, all features for the red-hued Tb (III) solution have identical peaks to that of the colorless solution, except for the two features at 696 $cm^{-1}$ and 672 $cm^{-1}$. According to Mu et al., these features are representative of the Tb-O-H stretch indicative of direct Tb-OH coordination.[61] With this data, the general structure predicted by EXAFS can be refined to $[Tb(CO_3)_3(OH)_3]^{6-}$, as illustrated in Figure 8e. Compared to the Tb (III) solid sample, both Tb (III) red-hued and colorless solution samples exhibit a blue shift by 30 $cm^{-1}$ to the band around 850 $cm^{-1}$ indicative of a change in carbonate coordination. This blue shift corresponds to increasing bond strength, which may be supporting evidence for a shift from monodentate to bidentate carbonate complexation.

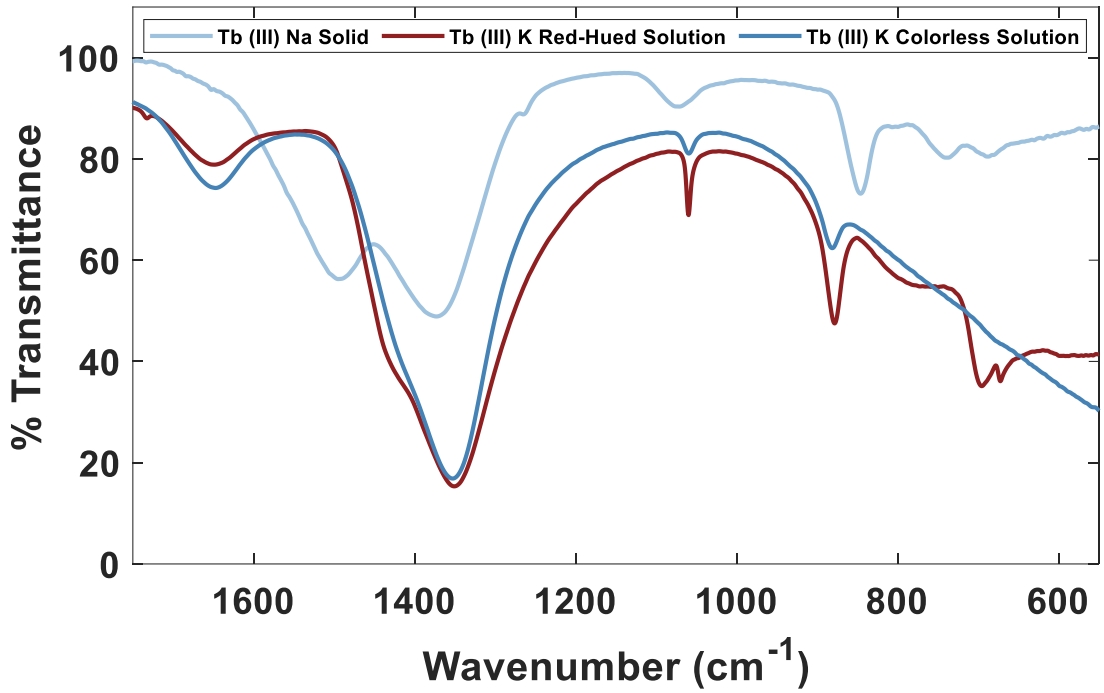


Figure 9: FT-IR data collected for Tb (III) solid (light blue), Tb (III) colorless solution (dark blue), and Tb (III) red-hued solution (red).

## Discussion

**Europium-$O_9$ versus terbium-$O_8$ coordination.** The change in speciation between the colorless Eu (III) and Tb (III) solution samples can be rationalized based upon the Ln-X distance differences for each shell. The distance differences between Eu-$O_9$ and Tb-$O_8$ (as well as for Ln-X, where X= $C_b$, $O_{dis}$, K) are all larger than 0.026 Å, which is the tabulated ionic radii difference between Eu and Tb (for CN = 8),[60] which are separated by only one element, gadolinium. Coincidentally, the majority of the distance differences in the solid samples, Eu-$O_9$ and Tb-$O_8$, are also above this tabulated value, despite only differing by one coordinated O atom and two distant Na ions. If both Eu and Tb had the same homleptic/heteroleptic coordination spheres, then the Ln-X distance differences would be equal to 0.026 Å (for X = O, $C_b$, $C_m$, $O_{dis}$, K/Na).[60] Since the majority of the experimentally observed distance differences are greater than 0.026 Å, this suggests that the speciation of the Eu (III) and Tb (III) carbonate complexes—despite being separated by Gd only—is not identical in the solids and solutions.

According to the model fits in Table 1, the basic structural unit for the Eu (III) and Tb (III) solid phases could be building blocks of coordination polymers in the solid state, a scenario that is seen in some structural and spectroscopic studies[62,63] of lanthanide carbonates across the 4f period. In each complex (solid and solution alike), we assume that any extra Ln-O not occupied by carbonate are a number of $OH^-$ anions and $H_2O$ molecules to complete the inner O coordination sphere. However, this is an assumption made, and our EXAFS results cannot detect protons (from

coordinated $OH^-$ or $H_2O$) and therefore, we are unable to decipher the exact water and hydroxide stoichiometries in the coordination complexes. The instrumental capability that would be useful and able to distinguish these two directly coordinated molecules is single crystal XRD, which we were not able to capture due to the inability to obtain suitable crystals.

Moreover, we must bear in mind the implications of the ± 1 atom statistical uncertainties (at the three-sigma level) for the coordination numbers of the distant cations on the stoichiometries of the coordination complexes. As such, we cannot definitively zero in on a single, charge-balanced anionic entity but, rather, the results lead to a few plausible molecular anions. Since the number of carbonates between the Tb and Eu solution complexes differ by 2 carbonates (equation 1, for Ln = Eu, Tb), it is more likely that the differing speciation is unique. The terbium solution system appears as strictly monodisperse as $[Tb(CO_3)_4]^{5-}$—in agreement with the speciation of Janicki et al.[26]. However, the solid complexes only differ by one carbonate ion complex which may exhibit a dynamical equilibrium reaction, such as equation 2. This equilibrium is shifted to the left for terbium and to the right for europium. The speciation for the Eu solution complex matched directly with the Mercier et al.[63] crystal structure with the substitution of K cations, and the Tb solid complex carbonate coordination matched directly with the Lin et al.[62] crystal structure with the substitution of Na cations.

$$[Ln(CO_3)_4]^{5-} + 2\,[CO_3]^{2-} \leftrightarrow\ [Ln(CO_3)_6]^{9-} \qquad \text{[eq 1]}$$

$$[Ln(CO_3)_5(H_2O)]^{7-} + 1\,[CO_3]^{2-} \leftrightarrow\ [Ln(CO_3)_6(H_2O)]^{9-} \qquad \text{[eq 2]}$$

Research published by Philippini et al.[35] studied the Dy (III) carbonate solution system, and they found no change in speciation between the Eu and Dy solutions. If the speciation of Eu (Z = 63) and Dy (Z = 66) are identical, then one would reasonably assume that the speciation for Tb (Z = 65) would also be the same and follow the trends outlined.[35] However, the EXAFS results reported here as well as the spectroscopic data of Janicki et al.[26] indicate that the Eu and Tb speciation are not identical, suggesting an equilibrium in solution proposed in equation 2. In support of equilibrium species, Vercouter et al. studied Ce (III) carbonate solutions and reported the tetra-carbonato 5- anion.[31]

**Solid versus solution structures.** The variations between the FT data for the solids and solutions (Figures 6 and 7) are significant, indicating changes in speciation upon dissolution of both Ln (III) salts. As reported by Janicki et al.,[26] their spectroscopic data for lanthanide carbonate complexes in solid and solution phases were "remarkably different". Notably, the increase of the most distant peak intensities in the FT are consistent with two phenomena: (1) an increase in the numbers of bidentate carbonate anions bound to the Ln (III) cations in the 5.5 M $K_2CO_3$ solutions, and (2) the presence of potassium ions in the outer spheres of the anionic carbonate complexes in the 5.5 M $K_2CO_3$ solutions. The $Na^+$ backscattering amplitude (in the solid salts) are weaker than that for the $K^+$ ions (in the solutions) (Figure S5). Therefore, distant Ln-Na correlations are weaker than the corresponding Ln-K ones. The anionic structural unit for the Eu (III) and Tb (III) solids are suggested as $[Eu(CO_3)_6(OH_n)]^{(y-9)}$ and $[Tb(CO_3)_5(OH_n)]^{(y-7)}$, respectively (for n = 1,2, y = n-2).

The Eu (III) solution speciation involves the homoleptic anion, e.g., $[Eu(CO_3)_6]^{9-}$. In alignment, the EXAFS results for the colorless Tb (III) solution is best described as the homoleptic anion $[Tb(CO_3)_4]^{5-}$. Compared with the corresponding solid phase complexes, the solution species have more bonded bidentate carbonate anions for Eu and Tb. This is also seen in the FT-IR spectra when Tb solid is compared to both Tb solution samples due to a blue shift in the carbonate band around 850 $cm^{-1}$. In each solution, we found evidence for either 4 or 5 K ions in the outer spheres of the Eu and Tb molecular anions, respectively, consistent with ion pairing. This difference in the distal peak between Figures 6 and 7 is most likely a combination of structural differences (through preferring bidentate coordination) and increased ion pairing interactions (1-2 additional cations).

Although the exact nature of the associations of the potassium ions with the anionic Ln (III) carbonate complexes in 5.5 M $K_2CO_3$ electrolytes is unknown, some insights can be drawn from the relatively shorter, 3.8-4.0 Å Ln (III)-K correlations. These are consistent with electrostatic contact ion pairing interactions, such as observed by small-angle X-ray scattering for Lindqvist hexaniobate salts, $A_8[Nb_6O_{19}]$ (A = Rb, Cs), dissolved in 3 M AOH solutions (as well as the ranges found in Table S10).[41,62,63] Another example, is that for lanthanum ferricyanide, $La[Fe(CN)_6]$, which upon dissolution in water forms strong contact ion-pairs between the $Fe(CN)_6^{3-}$ molecular anion and the La (III) cation at a nearly diffusion controlled rate.[64] More recently, D'Angelo et al. observed contact ion-pair formation with La (III) and nitrate anions in methanol solutions by use of XAS and MD simulations.[65] The remarkably strong amplitude of the La (III)−O−$N_{NO3-}$ correlation at 3.76 Å is comparable to the amplitude (and distance) of the Ln (III)-O-$C_{(CO3)}^{2-}$ interactions in our FT data of Figure 7.

**Terbium-$K_2CO_3$-$O_3$ solution system.** The colorless Tb (III) carbonate solution in 5.5 M $K_2CO_3$ darkened to a clear, red-hued color (see photograph, Figure 1) following the sparging of ozone gas through it. As stated in the results, when comparing the colorless Tb (III) solution to the red-hued Tb (III) solution, there is a decrease in the O CN from 8 to 6. The CN change correlates with a reduced Tb-O bond length, and the distance difference (0.12 Å) can be rationalized without resorting to a change of Tb valence. According to the ionic radii (IR) of Shannon,[60] the IR for Tb (III) with CN = 6 is 0.923 Å, whereas the IR for Tb (III) with CN = 8 is longer, 1.040 Å. The difference between these is 0.117 Å. That is, the Tb (III)-$O_6$ distance in the red-hued solution of Tb (III) should be 0.117 Å shorter than the Tb (III)-$O_8$ distance in the colorless solution of Tb (III). The EXAFS-determined bond length difference is essentially identical at 0.12 Å. This provides further proof that the valence of Tb in the red-hued solution is III. If Tb (IV) were present, based upon ionic radius arguments, the Tb (IV)-$O_6$ distance system is expected to be 0.28 Å shorter than the Tb (III)-$O_8$. Therefore, the XANES and EXAFS results independently indicate that—despite the color of the solution—there is no Tb (IV) observed in the red-hued solution obtained by ozonolysis. Furthermore, EPR results validated that only Tb (III) was present in the red-hued solution.

Given the rare nature of the formation and stabilization of Tb (IV), the achievements made in solid state materials are remarkable.[51,52,66] Several solids have been rigorously probed by others

using Tb $L_3$-edge XANES.[47,48,50,51] Whereas the XANES for Tb (III) is composed of one intense peak around +2.5 eV (Figures 3 and 4, Table S2), the XANES for Tb (IV) in the valence pure $TbO_2$ solid[47] is composed of one peak—with an unresolved shoulder on the leading edge—that is much weaker and at higher energy (with a maximum at +11.53 eV), than the peak for Tb (III) (Figure 5, Table S2). The Tb $L_3$-edge XANES for other valence-pure Tb (IV) solids, including $BaTbO_3$[48] and $SrTbO_3$,[48,49] are essentially equivalent to that for $TbO_2$. In contrast, the Tb $L_3$-edge XANES for the mixed valence (Tb (III)/(IV)) $Tb_4O_7$ solid[49,50] has two peaks centered at +3.53 and +11.53 eV (Figure 5, Table S2). The first peak corresponds to the Tb (III) response and the second to that for Tb (IV). The differences apparent in the Tb XANES shown in Figure 5 are typical of those expected for trivalent, mixed-valent, and tetravalent Tb. Curiously, in a recent report about a four-coordinate tetravalent terbium complex, Rice et al.[51] reported Tb $L_3$-edge XANES that suggest a mixed valent Tb (III/IV) system rather than a valence-pure tetravalent one. The reasons for the deviation from a typical Tb (IV) response, such as in Figure 5, are not known.

By comparison with the reference data for Tb (IV) solids, the Tb $L_3$-edge XANES for our solid salt as well as the two solutions (colorless and red-hued), see Figures 3 and 4, respectively, are diagnostic of Tb (III). Because the Tb XANES data is electronic in origin, the response is conclusive about the Tb (III) valence, even after ozonolysis. During ozonolysis, the function of ozone in this system is as an oxidant and, hence, it must be reduced, initially to the ozonide radical anion, $O_3^{-*}$ (* denotes radical ion), which subsequently decomposes to hydroxide through a cascade of reactions involving partially reduced oxygen species. The conundrum is the identification of the substrate that ozone acts upon to produce a color center. Unfortunately, the nature of the color center reported across many Tb literature sources could not be determined through XANES, EXAFS, EPR, and FT-IR. Conjecture on the nature of this color center is added to the SI, but future experimental work could be done to directly probe this phenomenon.

A second piece of information gained from the Tb XANES is insights into the identification of the coordination environment of Tb (III) in the red-hued solution. That is, the increased width of the edge peak was shown to arise from the overlap of 2p-5d transitions due to the ligand field splitting of the 5d orbitals in the presence of an octahedral coordination environment around the Tb (III) center. The second derivative of the XANES data, Figure 4b, confirms this by the two valleys seen in the red-hued solution and only a single valley seen for the colorless Tb (III) solution. If Tb (IV) were present in any of our materials, there would be changes in the edge peak shapes and positions as described elsewhere for the XANES of Tb (IV) (Figure 5). [47,48,50]

In further support of these findings, the analyses of the EXAFS reveal that the Tb (III)-O bond distance in the red-hued solution is significantly shorter than that in the colorless system. Although, this could be due to a difference in valence, wherein the higher oxidation state (IV) reveals a shorter distance than the lower (III) one, we demonstrated that the contraction is precisely accounted for the by change in coordination between the six-coordinate complex (red-hued solution) and the eight coordinate one (colorless solution). In line with the direct correlation between ionic radii and coordination numbers,[60] a complex with a CN = 6 will have a shorter bond

length than one with a CN = 8. These structure results provide further proof for the Tb (III) valence state in the red-hued sample following exhaustive ozonolysis.

# Conclusions

Through use of Eu and Tb $L_3$-edge XAS, we interrogated the Ln valences and coordination environments of solid carbonate complexes and their corresponding solution speciation. The XANES data demonstrated that all systems contained trivalent Ln ions, even the red-hued solution obtained by ozonolysis of the Tb (III)-$K_2CO_3$ electrolyte. Thus, contrary to many sources that reported colored Tb complexes as Tb (IV), indicating that not all colored Tb complexes are Tb (IV). The EXAFS data demonstrate that each of the Ln (III) cations formed molecular anions with inner-sphere carbonate and/or water (or hydroxide) coordination. The total carbonate complex speciation of the anionic Ln (III) carbonato complexes exhibits subtle variations between Eu and Tb solid samples. Moreover, the speciation of the solid Eu and Tb salts changes upon their dissolution in 5.5 M $K_2CO_3$. The solution samples exhibit features that have been interpreted as resulting from ion-pairing between the molecular carbonate complex anions and the potassium cations. This study also demonstrated through low temperature EPR analysis that the red color of the terbium carbonate solution obtained through the introduction of ozone gas is not due to the Tb (IV) valence state. Through XAS and FT-IR we were also able to observe a coordination shift in the different Tb (III) solution samples from eight-coordinate $[Tb(CO_3)_4]^{5-}$ (in the colorless solution) to an octahedral six-coordinate complex $[Tb(CO_3)_3(OH)_3]^{6-}$ (in the red-hued solution). Further spectroscopic and structure studies, both experimental and computational, are required to pinpoint the source of the color in the Tb-$K_2CO_3$-$O_3$ system. We hope that these results inform alkaline extraction and separation-based approaches by providing context in the form of carbonate speciation with Eu and Tb.

# Experiments

***Materials.*** Europium oxide (99.99%) was purchased from Treibacher Industrie AG. Terbium nitrate pentahydrate (99.9% trace metals basis), potassium hydroxide (90%), and potassium carbonate (99%) were purchased from Sigma Aldrich and used without purification. Sodium carbonate (ACS grade) was purchased from Fisher Scientific without purification. Ozone (35.2 $g/m^3$) was produced from an ozone generator (Oxidation Technologies, LLC, #VMUS-4) using high-purity oxygen gas at a flow rate of 6 liters per minute (purchased from General Air Supply).

***Synthesis.*** $Eu(NO_3)_3$ was synthesized from europium oxide by dissolving in concentrated nitric acid and evaporated to dryness. For the colorless Eu (III) and Tb (III) samples, concentrated solutions of sodium carbonate or potassium carbonate were added dropwise to the solutions of Ln (III) nitrate in excess nitric acid until no more precipitate formed. A vacuum filtration system was used to filter and thoroughly wash the white precipitates before drying in a vacuum oven. The solid Eu and Tb samples were measured by ICP-OES analysis (Perkin Elmer Avio 220 Max). The Eu

(III) solid sample had 6.12 wt% Na and 0.25 wt% K. The Tb (III) solid sample had 7.27 wt% Na and 0.10 wt% K.

We subjected colorless solutions of terbium (III) nitrate (43 mg, 0.098 mmol) dissolved in 7 mL of 5.5 M of $K_2CO_3$ with 0.1 M KOH to ozonolysis in efforts to oxidize Tb (III), providing access to Tb (IV). The colorless Tb (III) carbonate solution (7 mL) was placed in a glass vial with a bubbler hooked up to the ozone generator. Then, ozone was bubbled through the solution (12.67 g/hr) for 3 hours leading to a color change from colorless to red-orange depending upon the pathlength of the vial it is contained in. It is referred to as the 'red-hued Tb solution' throughout this paper. The UV-visible spectrum (CARY 500) of the freshly ozonized red-hued solution at equilibrium—as determined from the steady-state optical response—is shown as Figure 1 along with a photograph of the solution itself.

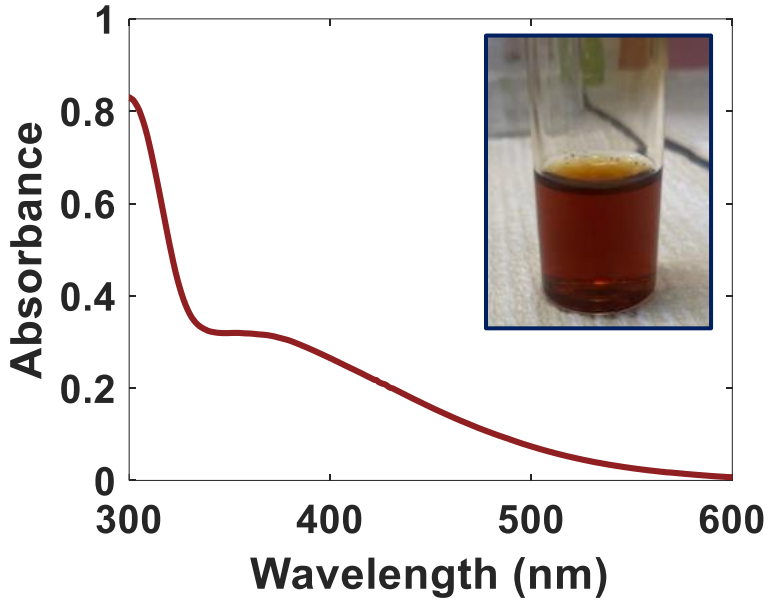


Figure 1: UV-Vis spectrum for red-hued Tb solution in 5.5 M $K_2CO_3$ following exhaustive ozonolysis. Spectrum obtained in a 1 cm pathlength cell.

***XAS measurements.*** All $L_3$-edge data were acquired at the Advanced Photon Source beam line (12-BM-B) at Argonne National Laboratory using conventional transmission and fluorescence detection as described elsewhere.[67] The incident X-ray energy was calibrated against the inflection point energy of an $Eu_2O_3$ film from EXAFS Materials Co. Each solution sample was contained in 1 mm diam. Kapton tubes that were sealed with epoxy. Each solid sample was prepared in an inert atmosphere glovebox and pressed into 0.015-inch-thick plastic washers sealed with Kapton tape-circles on both sides (purchased from McMaster-Carr, #95606A410). Transmission data was acquired for all solid samples ($1.1 \leq k \leq 10.9$ Å$^{-1}$) and fluorescence data was collected with a Vortex ME7 seven-element silicon drift detector for all liquid samples ($1.1 \leq k \leq 10.5$ Å$^{-1}$). Three 1 h scans were averaged for each specimen. All XANES data were normalized to unit edge jumps

and fitted in identical fashion using Athena,[68] see Supporting Information Tables S1-3. The EXAFS data were extracted from the primary experimental data by background subtraction using EXAFSPAK.[69] Analysis of the Ln $k^3\chi(k)$ EXAFS was performed with a fixed scale factor ($S_0^2$) of 0.9 for all solid and liquid samples. Single- and multi-shell curve fitting analyses were performed with EXAFSPAK (in *k*-space) and the recent release of WinXAS (version 4.02)–in *r*-space–using theoretical amplitude and phase function obtained from FEFF 8-Lite.[69,70] The available crystallographic structure information for sodium, potassium, and quaternary ammonium salts of lanthanide carbonates,[62,63,71] exhibit a number of bonding motifs. As shown in Figure S1 and Tables S4-S8, Ln (III) carbonate complexes can be either mononuclear molecular anions or extended polynuclear structures. In both, the carbonate bonding modes are either symmetric bidentate or monodendate, with or without additional water coordination, and with or without outer sphere alkali metal cations. All EXAFS data were fit using single-scattering (SS) and multiple-scattering (MS) pathways, with a conservative constraint, based upon the cluster fragment in illustrated Figure 2. All EXAFS datasets were fit with either 10–11 fitted variables (using one Debye-Waller term), which is less than the total number (17) of independent data points ($N_{idp}$) as estimated by $(2 \times \Delta k \times \Delta r)/\pi$.[72] The first O shell describes the inner sphere bonding (in terms of coordination number (CN), distance (r, Å) and Debye-Waller factor ($\sigma^2$, $Å^2$)) by all O ligands, which include contributions from monodentate and bidentate carbonate anions as well as possible contributions from bound hydroxide anions and water molecules (Table S9 and Figures S2-S3).[73] The second and third shells describe the C atoms in bidentate and monodentate coordination ($C_b$ and $C_m$, respectively). The last two shells are the distal (dis) O atoms and alkali metal cations (A ≡ Na, K), respectively. Based upon structure precedent (see Table S10), the $A^+$ ions can be sited at various positions (as illustrated in Figure S4), with Ln-A distances that are both shorter and longer than the Ln-$O_{dis}$ correlations. As required for bidentate coordination, the $O_{dis}$ CN was fixed to equal the $C_b$ CN; the corresponding Ln-$C_b$ and Ln-$O_{dis}$ distances were refined independently. The most distant shells in the coordination model of Figure 2 are necessary to account for the physically significant interactions visible in the FT data, particularly for the solution systems. Best Z fits were used to determine the atom origins of the outermost correlations, which were found to arise from the $O_{dis}$ atoms in combination with the $K^+$ ions for solutions and $Na^+$ ions for solids. Being separated by the 3rd period, the backscattering amplitude and phase functions for K (at the start of the 4th period) are quite distinct from those for the O and C atoms (near the end of the 2nd), see Figure S5(a). Also shown (Figure S5(c)) are the phase shift differences for the Ln-O and Ln-A as well as the Ln-Na and Ln-K scattering paths, the latter of which are approximately pi radians out of phase for $3 \leq k \leq 10$ $Å^{-1}$. Differences are also evident between the corresponding FEFF functions for Na, O, and C. Further information about the EXAFS analyses is provided in the Supplementary Information (SI) (Tables S11-S15). The FEFF input files for this analysis are also provided in the SI (File S1-S4).

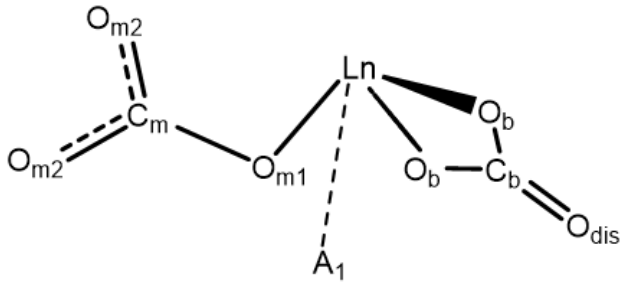


Figure 2: Structural motif based upon the crystallographic data in Table S10 showing monodentate and bidentate carbonate coordination and distant A atoms (with atom labels) as used to generate FEFF paths for the WinXAS fitting model. Full coordination complex model is illustrated in Figure S4.

***Electron Paramagnetic Resonance (EPR) Characterization.*** All EPR spectra were recorded on a Bruker EMXplus EPR equipped with a ColdEdge Stinger closed-cycle flow system to allow for low temperature measurements (Figure S6). The colorless Tb (III) carbonate and the red-hued Tb solutions were frozen directly in EPR tubes and each sample contained approximately 10 mM of Tb. The samples were preserved in liquid nitrogen until analyzed. To determine the oxidation states of Tb in both solutions, EPR spectra were recorded under the following conditions: temperature 5.6 K, modulation amplitude 8 G, microwave power 1.0 mW, and microwave frequency ~ 9.47 GHz. The spectra were simulated using EasySpin.[74]

***FT-IR measurements.*** All FT-IR spectra were recorded on a Thermo Scientific Nicolet iS50-FT-IR using the iS50 ATR. FT-IR was primarily used to determine the presence of Ln (III)-O-H coordination for the red-hued Tb (III) solution complex (Figure 9 and Figure S7).[61] For solution measurements, all samples were dried on the surface of the crystal prior to a measurement taken. The spectral resolution of the instrument was set to 2 $cm^{-1}$, and the ATR data were collected from 400 to 4000 $cm^{-1}$.

## Acknowledgments

The authors would like to thank our Mines colleague Dr Mark R. Antonio for his passion and force of XAS pedagogy, and his pantagruelian XAS efforts. This research was performed in part on beamline 12-BM-B at Sector 12 of the APS, a DOE Office of Science User Facility operated for the DOE Office of Science by Argonne National Laboratory, which is supported under Contract No. DE-AC02-06CH11357. The Colorado School of Mines authors acknowledge support by the Department of Energy/Basic Energy Science program under Award Number DE-SC0022217.

## TOC Graphic:

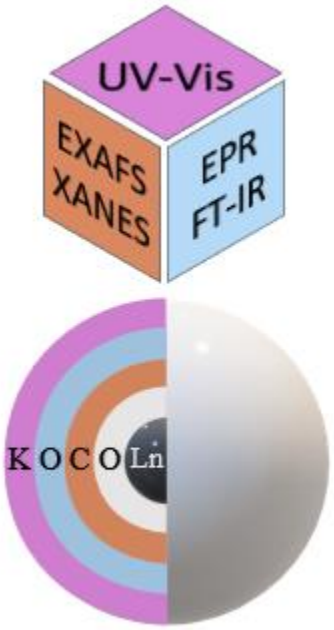


**TOC caption:** XAS revealed the formation of Eu(III) and Tb(III) molecular anions with inner-sphere, bidentate and monodentate carbonate and/or water (or hydroxide) coordination environments with outer-sphere contact ion-pairing that exhibit period variations and significant differences between the solid and solution speciation. After ozonolysis of a Tb(III)-$K_2CO_3$ solution, the UV-Vis, XAS, FT-IR, and EPR reveal a unique red-hued Tb(III) complex.

# References


[1] X. Wang, H. Chang, J. Xie, B. Zhao, B. Liu, S. Xu, W. Pei, N. Ren, L. Huang, W. Huang, *Coord Chem Rev* **2014**, *273–274*, 201–212, DOI 10.1016/J.CCR.2014.02.001.

[2] R. D. Teo, J. Termini, H. B. Gray, *J Med Chem* **2016**, *59*, 6012–6024, DOI 10.1021/acs.jmedchem.5b01975.

[3] M. Van de Voorde, K. Van Hecke, T. Cardinaels, K. Binnemans, *Coord Chem Rev* **2019**, *382*, 103–125, DOI 10.1016/J.CCR.2018.11.007.

[4] S. Cotton, *Lanthanide and Actinide Chemistry* **2006**, 1–263, DOI 10.1002/0470010088.

[5] F. Xie, T. A. Zhang, D. Dreisinger, F. Doyle, *Miner Eng* **2014**, *56*, 10–28, DOI 10.1016/J.MINENG.2013.10.021.

[6] U. Kesieme, A. Chrysanthou, M. Catulli, C. Y. Cheng, *Journal of Chemical Technology and Biotechnology* **2018**, *93*, 3374–3385, DOI 10.1002/jctb.5728.

[7] Z. K. Karalova, B. F. Myasoedov, T. I. Bukina, E. A. Lavrinovich, *Solvent Extraction and Ion Exchange* **1988**, *6*, 1109–1135, DOI 10.1080/07366298808917981.

[8] T. Litvinova, R. Kashurin, D. Lutskiy, *Materials* **2023**, *16*, 1–11, DOI 10.3390/ma16083140.

[9] M. E. De Vasconcellos, S. M. R. Da Rocha, W. R. Pedreira, C. A. Da, S. Queiroz, A. Abrão, *J Alloys Compd* **2006**, *418*, 200–203, DOI 10.1016/j.jallcom.2005.10.076.

[10] L. Brückner, T. Elwert, T. Schirmer, *Metals (Basel)* **2020**, *10*, 1–21, DOI 10.3390/met10010131.

[11] T. Taketatsu, *Bull Chem Soc Jpn* **1964**, *37*, 906–907, DOI 10.1246/bcsj.37.906.

[12] T. Taketatsu, *Bull Chem Soc Jpn* **1962**, *35*, 1573–1576, DOI 10.1246/bcsj.35.1573.

[13] H. S. Sherry, J. A. Marinsky, *Theory and Structure of Complex Compounds* **1964**, 339–348, DOI 10.1016/B978-1-4832-2841-9.50040-4.

[14] D. Edward Hobart, Electrochemical and Spectroscopic Studies of Some Less Stable Oxidation States of Selected Lanthanide and Actinide Elements, University of Tennessee, **1981**.

[15] P. Tse, N. P. Bessen, S. S. Galley, S. A. Bryan, A. M. Lines, J. Shafer, *J Electrochem Soc* **2022**, *169*, 046521, DOI 10.1149/1945-7111/AC6704.

[16] D. E. Hobart, K. Samhoun, J. P. Young, V. E. Norvell, G. Mamantov, J. R. Peterson, *Inorganic and Nuclear Chemistry Letters* **1980**, *16*, 321–328, DOI 10.1016/0020-1650(80)80069-9.

[17] M. O. Arman, B. Geboes, K. Van Hecke, K. Binnemans, T. Cardinaels, *J Appl Electrochem* **2022**, *52*, 583–593, DOI 10.1007/s10800-021-01651-0.

[18] R. C. Propst, *Journal of Inorganic and Nuclear Chemistry* **1974**, *36*, 1085–1094, DOI 10.1016/0022-1902(74)80218-6.

[19] P. G. Varlashkin, G. M. Begun, J. R. Peterson, *Journal of The Less-Common Metals* **1985**, *109*, 123–134, DOI 10.1016/0022-5088(85)90112-2.

[20] S. Qiang, W. Zhijian, G. Chongli, *Solvent Extraction and Ion Exchange* **1995**, *13*, 275–288, DOI 10.1080/07366299508918274.

[21] Y. M. So, W. H. Leung, *Coord Chem Rev* **2017**, *340*, 172–197, DOI 10.1016/j.ccr.2016.12.009.

[22] K. Binnemans, *Applications of Tetravalent Cerium Compounds*, Leuven, Belgium, **2006**, ISBN DOI 10.1016/S0168-1273(06)36003-5.

[23] N. A. Piro, J. R. Robinson, P. J. Walsh, E. J. Schelter, *Coord Chem Rev* **2014**, *260*, 21–36, DOI 10.1016/j.ccr.2013.08.034.

[24] E. Allahkarami, B. Rezai, *J Environ Chem Eng* **2021**, *9*, 1–20, DOI 10.1016/j.jece.2020.104956.

[25] G. T. Seaborg, *Radiochim Acta* **1993**, *61*, 115–122, DOI 10.1524/ract.1993.61.34.115.

[26] R. Janicki, P. Starynowicz, A. Mondry, *Eur J Inorg Chem* **2011**, 3601–3616, DOI 10.1002/ejic.201100184.

[27] W. Runde, C. Van Pelt, P. O. Allen, *J Alloys Compd* **2000**, *303–304*, 182–190, DOI 10.1016/S0925-8388(00)00665-4.

[28] V. Philippini, T. Vercouter, A. Chaussé, P. Vitorge, *J Solid State Chem* **2008**, *181*, 2143–2154, DOI 10.1016/j.jssc.2008.04.030.

[29] W. Runde, M. P. Neu, C. Van Pelt, B. L. Scott, *Inorg Chem* **2000**, *39*, 1050–1051, DOI 10.1021/ic991087w.

[30] R. Janicki, P. Lindqvist-Reis, *Dalton Transactions* **2018**, *47*, 2393–2405, DOI 10.1039/c7dt04836j.

[31] T. Vercouter, P. Vitorge, N. Trigoulet, E. Giffaut, C. Moulin, *New J. Chem.* **2005**, *29*, 544–553, DOI 10.1039/b413002b.

[32] F. Martelli, Y. Jeanvoine, T. Vercouter, C. Beuchat, R. Vuilleumier, R. Spezia, *Physical Chemistry Chemical Physics* **2014**, *16*, 3693–3705, DOI 10.1039/c3cp54001d.

[33] M. Duvail, P. Vitorge, R. Spezia, *Journal of Chemical Physics* **2009**, *130*, 104501, DOI 10.1063/1.3081143.

[34] B. Taravel, F. Fromage, P. Delorme, V. Lorenzelli, *J Mol Struct* **1973**, *16*, 483–498, DOI 10.1016/0022-2860(73)80115-2.

[35] V. Philippini, T. Vercouter, P. Vitorge, *J Solution Chem* **2010**, *39*, 747–769, DOI 10.1007/s10953-010-9539-4.

[36] V. Philippini, T. Vercouter, J. Aupiais, S. Topin, C. Ambard, A. Chaussé, P. Vitorge, *Electrophoresis* **2008**, *29*, 2041–2050, DOI 10.1002/elps.200700764.

[37] C. Riglet-Martial, P. Vitorage, V. Calmon, *Radiochim. Acta* **1998**, *82*, 69–76, DOI 10.1524/ract.1998.82.special-issue.69.

[38] N. Larabi-Gruet, A. Chaussé, L. Legrand, P. Vitorge, *Electrochim Acta* **2007**, *52*, 2401–2410, DOI 10.1016/j.electacta.2006.08.046.

[39] F. A. Cotton, G. Wilkinson, C. A. Murillo, M. Bochmann, *Advanced Inorganic Chemistry*, John Wiley & Sons, New York, **1999**.

[40] Y. Marcus, G. Hefter, *Chem Rev* **2006**, *106*, 4585–4621, DOI 10.1021/cr040087x.

[41] M. R. Antonio, M. Nyman, T. M. Anderson, *Angewandte Chemie International Edition* **2009**, *48*, 6136–6140, DOI 10.1002/anie.200805323.

[42] F. W. Lytle, G. Van Der Laan, R. B. Greegor, E. M. Larson, C. E. Violet, J. Wong, *Phys. Rev. B* **1990**, *41*, 8955–8963, DOI 10.1103/PhysRevB.41.8955.

[43] M. R. Antonio, L. Soderholm, A. J. G. Ellison, *J Alloys Compd* **1997**, *250*, 536–540, DOI 10.1016/S0925-8388(96)02736-3.

[44] C. E. Housecroft, A. G. Sharpe, *Inorganic Chemistry*, Pearson, Harlow, **2012**.

[45] M. Winter, The Orbitron, University of Sheffield, https://winter.group.shef.ac.uk/orbitron/.

[46] A. D. Braatz, M. R. Antonio, M. Nilsson, *Dalton Transactions* **2017**, *46*, 1194–1206, DOI 10.1039/c6dt04305d.

[47] S. G. Minasian, E. R. Batista, C. H. Booth, D. L. Clark, J. M. Keith, S. A. Kozimor, W. W. Lukens, R. L. Martin, D. K. Shuh, S. C. E. Stieber, T. Tylisczcak, X. D. Wen, *J Am Chem Soc* **2017**, *139*, 18052–18064, DOI 10.1021/jacs.7b10361.

[48] K. Ueda, Y. Shimizu, K. Nagamizu, M. Matsuo, T. Honma, *Inorg Chem* **2017**, *56*, 12625–12630, DOI 10.1021/acs.inorgchem.7b02165.

[49] U. Staub, M. R. Antonio, L. Soderholm, M. Guillaume, W. Henggeler, A. Furrer, *Phy. Rev. B* **1994**, *50*, 7085–7091, DOI 10.1103/PhysRevB.50.7085.

[50] U. Staub, L. Soderholm, S. Skanthakumar, M. R. Antonio, *Journal De Physique IV Colloque* **1997**, *7*, 1077–1079, DOI 10.1051/jp4:19972141.

[51] N. T. Rice, I. A. Popov, D. R. Russo, J. Bacsa, E. R. Batista, P. Yang, J. Telser, H. S. La Pierre, *J Am Chem Soc* **2019**, *141*, 13222–13233, DOI 10.1021/jacs.9b06622.

[52] C. T. Palumbo, I. Zivkovic, R. Scopelliti, M. Mazzanti, *J Am Chem Soc* **2019**, *141*, 9827–9831, DOI 10.1021/jacs.9b05337.

[53] T. Xue, Y. S. Ding, X. L. Jiang, L. Tao, J. Li, Z. Zheng, *Precision Chemistry* **2023**, *1*, 583–591, DOI 10.1021/prechem.3c00065.

[54] T. P. Gompa, S. M. Greer, N. T. Rice, N. Jiang, J. Telser, A. Ozarowski, B. W. Stein, H. S. La Pierre, *Inorg Chem* **2021**, *60*, 9064–9073, DOI 10.1021/acs.inorgchem.1c01062.

[55] J. McPeak, D. Alexander, C. Joseph, S. S. Eaton, G. R. Eaton, *Appl Magn Reson* **2020**, *51*, 961–976, DOI 10.1007/s00723-020-01262-6.

[56] M. R. Gafurov, V. A. Ivanshin, I. N. Kurkin, M. P. Rodionova, H. Keller, M. Gutmann, U. Staub, *Journal of Magnetic Resonance* **2003**, *161*, 210–214, DOI 10.1016/S1090-7807(03)00002-8.

[57] R. J. Ellis, Y. Meridiano, R. Chiarizia, L. Berthon, J. Muller, L. Couston, M. R. Antonio, *Chem. Eur. J.* **2013**, *19*, 2663–2675, DOI 10.1002/chem.201202880.

[58] T. Ressler, **2023**.

[59] T. Ressler, *J Synchrotron Radiat* **1998**, *5*, 118–122, DOI 10.1107/S0909049597019298.

[60] R. D. Shannon, *Acta Cryst.* **1976**, *A32*, 751–767, DOI 10.1107/s0567739476001551.

[61] Q. Mu, Y. Wang, *J Alloys Compd* **2011**, *509*, 2060–2065, DOI 10.1016/j.jallcom.2010.10.141.

[62] Y. Lin, C. L. Hu, Z. Fang, J. Chen, W. J. Xie, Y. Chen, J. P. Wang, J. G. Mao, *Inorg Chem Front* **2022**, *9*, 5645–5652, DOI 10.1039/d2qi01533a.

[63] N. Mercier, M. Leblanc, E. Antic-Fidancev, M. Lemaitre-Blaise, *J Solid State Chem* **1997**, *132*.

[64] R. Buchner, J. Barthela, B. Gillb, *Phys. Chem. Chem. Phys.* **1999**, *1*, 105–109, DOI 10.1039/A806795C.

[65] P. D'Angelo, V. Migliorati, A. Gibiino, M. Busato, *Inorg Chem* **2022**, *61*, 17313–17321, DOI 10.1021/acs.inorgchem.2c02932.

[66] T. P. Gompa, A. Ramanathan, N. T. Rice, H. S. La Pierre, *Dalton Transactions* **2020**, *49*, 15945–15987, DOI 10.1039/d0dt01400a.

[67] E. R. Bertelsen, N. C. Kovach, B. J. Reinhart, B. G. Trewyn, M. R. Antonio, J. C. Shafer, *CrystEngComm* **2020**, *22*, 6886–6899, DOI 10.1039/d0ce00956c.

[68] B. Ravel, M. Newville, *J Synchrotron Radiat* **2005**, *12*, 537–541, DOI 10.1107/S0909049505012719.

[69] G. N. George, I. J. Pickering, **2000**.

[70] J. J. Rehr, A. Ankudinov, B. Ravel, User's Guide, FEFF v8.40, University of Washington, **2006**.

[71] R. Janicki, P. Starynowicz, A. Mondry, *Eur J Inorg Chem* **2011**, 3601–3616, DOI 10.1002/ejic.201100184.

[72] J. E. Penner-Hahn, *X-Ray Absorption Spectroscopy*, **2003**.

[73] C. Hennig, A. Ikeda-Ohno, F. Emmerling, W. Kraus, G. Bernhard, *Dalton Transactions* **2010**, *39*, 3744–3750, DOI 10.1039/b922624a.

[74] S. Stoll, A. Schweiger, *Journal of Magnetic Resonance* **2006**, *178*, 42–55, DOI 10.1016/j.jmr.2005.08.013.